

Cardiac troponin T mutations result in allele-specific phenotypes in a mouse model for hypertrophic cardiomyopathy

Jil C. Tardiff,^{1,2} Timothy E. Hewett,³ Bradley M. Palmer,⁴ Charlotte Olsson,⁴ Stephen M. Factor,⁵ Russell L. Moore,⁴ Jeffrey Robbins,³ and Leslie A. Leinwand¹

¹Department of Molecular, Cellular and Developmental Biology, University of Colorado, Boulder, Colorado 80309, USA

²Division of Cardiology, Albert Einstein College of Medicine, Bronx, New York 10461, USA

³Department of Pediatrics, Division of Molecular Cardiovascular Biology, Children's Hospital Research Foundation, Cincinnati, Ohio 45229, USA

⁴Department of Kinesiology and Applied Physiology, University of Colorado, Boulder, Colorado 80309, USA

⁵Department of Medicine, Albert Einstein College of Medicine, Bronx, New York 10461, USA

Address correspondence to: Leslie A. Leinwand, Department of Molecular, Cellular and Developmental Biology, University of Colorado, Campus Box 347, Boulder, Colorado 80309, USA. Phone: (303) 492-7606; Fax: (303) 492-8907; E-mail: leinwand@stripe.colorado.edu.

Received for publication December 15, 1998, and accepted in revised form July 1, 1999.

Multiple mutations in cardiac troponin T (cTnT) can cause familial hypertrophic cardiomyopathy (FHC). Patients with cTnT mutations generally exhibit mild or no ventricular hypertrophy, yet demonstrate a high frequency of early sudden death. To understand the functional basis of these phenotypes, we created transgenic mouse lines expressing 30%, 67%, and 92% of their total cTnT as a missense (R92Q) allele analogous to one found in FHC. Similar to a mouse FHC model expressing a truncated cTnT protein, the left ventricles of all R92Q lines are smaller than those of wild-type. In striking contrast to truncation mice, however, the R92Q hearts demonstrate significant induction of atrial natriuretic factor and β -myosin heavy chain transcripts, interstitial fibrosis, and mitochondrial pathology. Isolated cardiac myocytes from R92Q mice have increased basal sarcomeric activation, impaired relaxation, and shorter sarcomere lengths. Isolated working heart data are consistent, showing hypercontractility and diastolic dysfunction, both of which are common findings in patients with FHC. These mice represent the first disease model to exhibit hypercontractility, as well as a unique model system for exploring the cellular pathogenesis of FHC. The distinct phenotypes of mice with different TnT alleles suggest that the clinical heterogeneity of FHC is at least partially due to allele-specific mechanisms.

J. Clin. Invest. 104:469-481 (1999).

Introduction

Familial hypertrophic cardiomyopathy (FHC) is a dominant disease of the cardiac sarcomere. Mutations in many components of the thick and thin filaments have been identified, including the β -myosin heavy chain (β -MyHC), both myosin light chains, myosin-binding protein C tropomyosin (α -TM), cardiac troponin T (cTnT), and troponin I (TnI) (1). Thus, the disease is genetically heterogeneous. The types of mutations that have been found in the genes are also quite varied. For example, most of the mutations in the β -MyHC are missense mutations, whereas mutations in the cTnT and myosin-binding protein C genes can be splice-site mutations, deletions of codons, and missense mutations. The disease is also clinically heterogeneous, with some mutant alleles resulting in a poor clinical prognosis, whereas others are associated with a good prognosis (2). In general, mutations in the β -MyHC gene are associated with moderate to severe ventricular hypertrophy and variable sudden death, whereas mutations in cTnT are associated with mild or no hypertrophy and a high incidence of sudden death. The fact that all the mutations implicated in this disease are in genes encoding sarcomeric proteins has led to the suggestion that the pathogenesis of the disease likely involves a common mechanism of contractile dysfunction.

Several approaches have been used to understand mechanisms of pathogenesis, as well as the basis for the observed clinical heterogeneity. In vitro biochemical approaches have demonstrated that mutations in the β -MyHC function through a dominant negative mechanism and that several mutants have defects in actin-activated ATPase activity (3-5). This reduction in motor activity presumably triggers a compensatory hypertrophic response, explaining the high frequency of hypertrophy in patients with MyHC mutations. Transgenic mouse models have been created for mutations in the cardiac MyHC, and these models have both similarities and differences with each other and with the human disease. Both models exhibit many of the histological features of the disease; one exhibits significant ventricular hypertrophy, whereas the other exhibits no ventricular hypertrophy (6,7).

Structurally, cTnT interacts directly with TM along extended regions that span the head-to-tail region of the contiguous array of TMs within the thin filament and is thought to promote the ordered assembly of the Tn-TM complex onto the actin filament (8). The 3' end of the molecule also binds the TnI-TnC complex. In low-Ca²⁺ states (relaxation), TnT binding to TnI-TnC allows the inhibition of the myofibrillar actomyosin

MgATPase by TnI. This effect is overcome at higher $[Ca^{2+}]$ (contraction), where the binding of Ca^{2+} to TnC favors the reformation of the permissive TnI-TnC complex (9). Thus, the ability of the thin filament to respond to shifts in Ca^{2+} within the myocyte is modulated by multiple protein-protein interactions that occur along the cTnT molecule. Both skeletal and cardiac muscle TnT are expressed as multiple isoforms, and it has been postulated that this allows flexibility in adapting to physiological changes. Since the initial mapping of the cTnT-related FHC alleles in 1994, several *in vitro* studies have been performed using human and rat cTnT alleles in an attempt to better understand the effects of these mutations at the level of the cardiac sarcomere (10). Using a primary quail myocyte culture system in transfection studies, Watkins et al. (11) were able to demonstrate that full replacement of the native quail TnT with a truncated form of human cTnT (deletion of exon 15) resulted in a much-diminished maximal force of contraction. The mechanism of this decrease in Ca^{2+} -activated maximum force remains unclear, although it is possible that this effect is due to an alteration in the Ca^{2+} sensitivity of the thin filament caused by the partial deletion of the TM-TnI-TnC binding site. Point mutations in the TM binding site (I79N and R92Q) have been studied in a variety of systems, including adenovirus infection of feline cardiac myocytes, *in vitro* reconstitution assays, and cTnT exchange studies using permeabilized rabbit cardiac muscle fibers (12–14). Although the results have varied depending on the experimental system, several key observations have emerged, including decreased contractile performance, increased thin filament sliding speed in an *in vitro* motility assay, and increased Ca^{2+} sensitivity. In particular, it appears that point mutations in the TM binding site do not result in changes in maximal force-generating capability (14). This is in contrast to *in vitro* studies performed on several of the β -MyHC alleles, wherein the observed contractile impairment has been postulated to result in a compensatory hypertrophic response (15). Most recently, 3 additional cTnT-related FHC alleles were analyzed in transfected quail skeletal myotubes (I79N, R92Q, and Δ 160). All 3 mutants showed a decreased Ca^{2+} sensitivity of force production, whereas a subset (I79N and R92Q) exhibited an increased velocity of shortening (16). The reason for this difference in Ca^{2+} sensitivity in 2 different studies is unclear and will likely require additional experimentation.

We recently described a transgenic mouse model for the truncated allele of cTnT and found that the hearts of these animals develop a severe cardiomyopathy with significant myocellular disarray but no apparent fibrosis (17). Surprisingly, the hearts of these animals are significantly smaller than those of controls. The reduction in ventricular mass could be explained by the observation that there are fewer myocytes and that those that are there are smaller than controls. In addition, the hearts develop severe diastolic dysfunction and milder, but significant, systolic dysfunction. Although no reports of sudden death in the mutant MyHC mice have been reported, mice that express approximately 10% of their

cTnT as the truncation mutant die within 8 hours of birth. In contrast, a recent report of a transgenic mouse expressing a different allele of cTnT (R92Q) demonstrated no alterations in chamber dimension or systolic function, but a reduction in diastolic function when hearts contain 1–10% of their cTnT as this mutant (18). We report here significantly different findings, with mice expressing 30%, 67%, and 92% of their cTnT as the same R92Q mutant allele. Just as in the case of the truncated cTnT allele, the hearts of these animals are significantly smaller than those of controls. In contrast, they exhibit significant dose-dependent fibrosis. They also demonstrate enhanced systolic function in the presence of diastolic dysfunction, consistent with the hypothesis that at least some TnT mutant alleles result in a hypercontractile heart. While hypercontractility is a common finding in patients with FHC (19,20), the cause remains unclear, and these animals provide clear insight into that phenotype, as we show here that the cells themselves are hypercontractile. In addition, electron micrographic analysis demonstrates little degeneration of the myofibrils but, instead, gross alterations in mitochondrial morphology and increases in mitochondrial numbers along with lipid deposition. These ultrastructural findings are distinct from those of the hearts of mice expressing the truncated TnT allele, which show myofibrillar disarray.

Methods

Clone construction and screening. A full-length (1,089 nucleotide) adult mouse cTnT cDNA clone was isolated from a BALB/c mouse cardiac λ gt11 cDNA library (CLONTECH Laboratories Inc., Palo Alto, California, USA) and cloned into Bluescript KS⁺ (Stratagene, La Jolla, California, USA). The full-length cDNA (WT) was tagged at the NH₂-terminus with an 11-amino acid human *c-myc* epitope by PCR using Vent DNA Polymerase (New England Biolabs Inc., Beverly, Massachusetts, USA) (21). The 5' oligonucleotide (containing sequence for the *c-myc* tag and *MluI-EcoRI* restriction sites) ACGCGTGAATTCTAATGGTGGAGCAAAGCTCATTTCTGAAGAGGAGGACTTGTCTGACGCCGAGGAGGTGGTG was paired with the 3' oligonucleotide CCGAAGCTTTCATCATTTCCAACGCCCGGTGACTTTG. The resultant DNA fragment was subcloned into Bluescript, and the sequence was verified by Thermal Cycle sequencing. The R92Q construct was generated by oligonucleotide mutagenesis. A 5' internal oligonucleotide including a naturally occurring *Bsu36I* site was paired with a 3' oligo containing both a dinucleotide missense mutation and an internal *AlwNI* restriction site. A 220-bp internal fragment was generated by PCR and *Pfu* polymerase (Stratagene) using the WT-Bluescript clone as a template. The resultant fragment was subcloned into PCR-Blunt (Invitrogen Corp., Carlsbad, California, USA), sequenced, and reisolated as a *Bsu36I-AlwNI* fragment. The original WT-Bluescript construct was digested with *Bsu36I* and *AlwNI* to isolate the 2 fragment arms and then gel purified. The internal R92Q fragment was ligated to 2 fragments isolated as just described in a 3-part ligation to produce in a 5' *myc*-tagged R92Q construct (R92Q-Myc). The R92Q-Myc Bluescript construct was digested with *MluI-EcoRV*, and

the isolated fragment was ligated to a preexisting vector containing -2,996 bp of 5' upstream sequence from the rat α -MyHC promoter and 1,500 bp of the mouse β^{maj} globin terminator separated by a multiple cloning site (22). The resultant transgene constructs are digested with *KpnI* to isolate a 5.5-kb linear fragment and used in microinjections. The transgene was injected into the pronuclei of CBA/B6 fertilized mouse eggs derived from an F1 cross between FVB/N and C57/B6 strains (23). Founders were screened by Southern analysis of tail DNA using a 650-bp internal transgene probe. All F1 and subsequent screenings are performed by PCR using a pair of transgene-specific primers: 5' (α Promoter) ACCTAGAGGGAAAGTGTCTT and 3' (Myc-TnT) TCCTCTTCAGAGATGAGCTTT. All PCR reactions contained the internal control housekeeping primers *Mus1* (TGAGGTTGCTTCTGATCTGC) and *Mus2* (TCCTGGACAAAGTAACCCTTG).

Cardiac protein isolation and Western analysis. Crude cardiac protein and myofibril isolation and subsequent SDS-PAGE/Western analysis were performed as described previously (17).

Ultrastructural analysis. Five-week-old mice were sacrificed, and the hearts were immediately excised and rinsed in ice-cold PBS + 1 mM EDTA. Each heart was successively immersed in 10, 20, and 30% ice-cold sucrose solution (wt/vol in PBS + 1 mM EDTA) for 15 minutes (each step) on ice. Hearts were taken from the 30% sucrose solution, cut into small blocks, and immediately transferred to fresh ice-cold 4% paraformaldehyde and 1% glutaraldehyde in 0.1 M PBS with 5% sucrose (wt/vol) for 24 hours. The tissue was washed several times in buffer and postfixed for 1 hour in 1% osmium tetroxide. After several rinses in buffer, the tissue was dehydrated in ascending ethanol solutions, cleared in acetonitrile, and infiltrated in a mixture of Araldite-Epon. The tissue blocks were subsequently flat-embedded. Toluidine blue-stained sections (1 μm) were first examined by light microscopy, and well-oriented (longitudinal) tissue blocks were then cut for thin sections, stained with uranyl-acetate and lead-citrate, and examined with a JEOL-100CX electron microscope (JEOL USA Inc., Cranford, New Jersey, USA).

Northern analysis. Isolation of total RNA from mouse hearts was performed as described by Chomczynski and Sacchi (24). A total of 10 μg of total RNA from each source was separated on an 0.8% agarose-formaldehyde gel, transferred to a nylon membrane (ICN Biochemicals Inc., Costa Mesa, California, USA), and sequentially hybridized with a series of radiolabeled DNA probes. Unique single-stranded oligonucleotide sequences corresponding to α -MyHC (5'-GAGGGTCTGCTGGAGAGG-3') and β -MyHC (5-TGTTGCAAAGGCTCCAGGTCTGAGGGCTTC-3') were end-labeled and added to hybridization solution composed of 7% SDS, 10 \times Denhardt's solution, 20 mM NaPO₄ (pH 7.2), 5 \times SSC, and 0.2 mg/mL denatured salmon sperm DNA. The blots were hybridized overnight at 55 $^{\circ}\text{C}$. Sequential washes were performed (2 \times SSC/0.1% SDS, 1 \times SSC/0.1% SDS, 0.5 \times SSC/0.1% SDS) at 42 $^{\circ}\text{C}$, and the blots were exposed overnight with an intensifying screen at -70 $^{\circ}\text{C}$. Restriction fragments of GAPDH, atrial natriuretic factor (ANF), murine cTnT, and SERCA2 cDNA

sequence were isolated and labeled by random priming. Hybridizations were performed overnight at 65 $^{\circ}\text{C}$ in the following hybridization solution: 5 \times SSC, 1 \times Denhardt's solution, 10% dextran sulfate, 50% formamide, 1% SDS, and 0.2 mg/mL denatured salmon sperm DNA. Washes were performed as already described at 65 $^{\circ}\text{C}$ and with an added wash with 0.1 \times SSC/0.1% SDS. Blots were exposed overnight with an intensifying screen at -70 $^{\circ}\text{C}$.

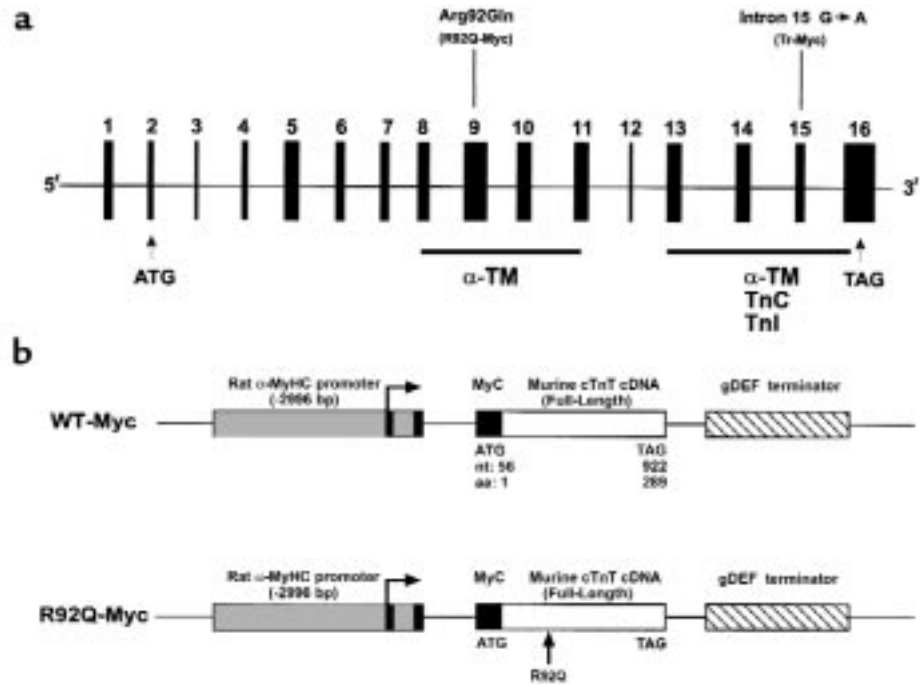
Isolated perfused working heart preparation. These studies were carried out as described previously (17).

Adult cardiac myocyte isolation. Ventricular cardiocytes were obtained from control, wild-type, and transgenic mice using a modification of the protocol described by Wolska and Solaro (25). All chemical and reagents were obtained from Sigma Chemical Co. (St. Louis, Missouri, USA) except as noted. Mice were heparinized (250 U, intraperitoneally) 15 minutes before administration of an anesthetic dose of sodium pentobarbital (35 mg/kg body weight, intraperitoneally; Abbott Laboratories, North Chicago, Illinois, USA). Under deep anesthesia, hearts were exposed by midline thoracotomy and were rapidly excised and placed in ice-cold (0-2 $^{\circ}\text{C}$) saline solution. An 18-gauge stainless steel cannula was fixed in the aorta with 6-0 surgical silk suture, and each heart was retrogradely perfused (75 cmH₂O perfusion pressure) with an oxygenated (95% O₂/5% CO₂) nominal Ca²⁺-containing modified Krebs-Henseleit (KH) buffer (pH 7.4, 37 $^{\circ}\text{C}$) for 4 minutes. Hearts were then perfused (45 cmH₂O perfusion pressure) for an additional 10-15 minutes with a similar modified KH buffer that contained collagenase (375 U/mL; Worthington Biochemical Corp., Lakewood, New Jersey, USA) and 50 μM CaCl₂. Hearts were removed from the cannula, and the atria and aorta were trimmed away and discarded. The remaining left and right ventricular myocardium was minced and mechanically agitated for 6-8 minutes in modified KH buffer (37 $^{\circ}\text{C}$, pH 7.4) containing 100 μM CaCl₂. The resulting cell suspension was gently subjected to 7-10 passes through a 10-mL plastic culture pipette and was filtered through a 250- μm nylon mesh filter. A total of 10 mM 2,3-butanedionemonoxime (BDM) was present in all perfusates and cell isolation buffers throughout the protocol. Cells from each experimental group were divided into 2 aliquots and allowed to passively settle for 7 minutes. One cell pellet was resuspended in a bicarbonate-based Medium 199, and the other pellet was resuspended in Medium 199 containing 10 mM BDM. Cell suspensions were then plated onto laminin-coated glass coverslips and incubated for 2-8 hours at 37 $^{\circ}\text{C}$ with 5% CO₂/20% O₂.

Cell morphology and myocyte-shortening dynamics. Coverslips from each experimental group (control, wild-type, and transgenic) and subgroup (+/- BDM) were microscopically examined (Nikon Diaphot, $\times 40$ lens; Nikon Corp., Melville, New York, USA), and images of cardiocytes were recorded onto videotape. Video images of individual cardiocytes were analyzed for maximal length, midpoint width, and area using Image 1.41 software (National Institutes of Health, Bethesda, Maryland, USA). To assess myocyte-shortening dynamics, additional coverslips (Medium 199 without BDM) were used to form the bottom of a custom-built flow-through chamber (26). The chamber was placed on the stage of

Figure 1

R92Q-TnT and truncation-TnT map to 2 distinct functional domains. (a) Exon composition of human cTnT, with positions of disease alleles Arg92Gln and intron 15 G→A marked above. The representative murine transgene allele is in parenthesis below. Functional domains are depicted by filled bars, with associated protein binding sites below. Location of translational start and stop codons are represented by ATG and TAG, respectively. (b) Constructs used to generate wild-type (WT) and Arg92Gln (R92Q) Myc-tagged murine cardiac TnT.



an inverted microscope (Nikon Diaphot) fitted with a $\times 40$ oil-immersion objective (Fluor 40, numerical aperture = 1.30). Coverslips were superfused with a normal Tyrodes solution (in mM: 140 NaCl, 6 KCl, 1 MgCl₂, 2 CaCl₂, 10 glucose, 2 pyruvate, and 5 HEPES [pH 7.4]) and maintained at 29°C. Cardiocytes were electrically paced at 0.5 Hz by field stimulation using platinum electrodes with a 0.5-microsecond stimulus duration at an intensity of 1.5 \times threshold. Myocyte contractile activity was assessed by video edge detection (Crescent Electronics, Sandy, Utah, USA) and recorded using an A-to-D converter and a microcomputer. Custom-made software was used to analyze cardiocyte-shortening transients, and the following characteristics were analyzed: maximal extent of shortening, time to peak shortening, maximal shortening and relengthening velocities ($\mu\text{m/s}$), maximal rates of shortening and relengthening (s^{-1}), and time to 50% relaxation. Sarcomere lengths were assessed from white-light video images taken using a Nikon $\times 100$ oil-immersion lens equipped with commercially available software (IonOptix Corp., Milton, Massachusetts, USA).

Statistical analysis. The myocyte morphology data were analyzed using a 2-way (group \times BDM) ANOVA. Myocyte-shortening data were analyzed using a 1-way ANOVA. In both types of analyses, statistical differences were identified at the $P < 0.05$ and $P < 0.10$ levels. The latter significance criterion was used following the principles described by Williams et al. (27). Briefly, examination of data at the $P < 0.10$ level reduces the probability of committing a type II error (accepting the null hypothesis when it is false), and may be more appropriate for exploratory (rather than confirmatory) investigation. In our statistical analysis, we ascribed to the principle that in an investigation of myocyte properties, myocytes serve as the best proxy to themselves. This approach maximizes statistical power and enhances the chance of detecting between group dif-

ferences, but it does so at the expense of strictly satisfying the data sampling independence assumption. Strict satisfaction of the sampling independence assumption could have only been achieved had we (a) been able to pool cells from all the hearts used in the study and sampled from a common pool or (b) used hearts as the unit of analysis. The former option was not technically practical and would have resulted in a marked reduction in the number of cells we could have sampled. The latter option would have created an analytical scenario in which we would have had virtually no statistical power and would have assumed a large exposure to type II errors.

Results

Generation of R92Q-Myc transgenic mice. All the known cTnT-related FHC alleles in humans map within 2 major functional domains (28,29). Our previously described cTnT-FHC transgenic mouse model demonstrated the pathophysiological effects of disrupting the COOH-terminal α -TM-TnI-TnC binding domain of cTnT (17). To determine whether mutations in different functional domains could account for some of the diverse clinical phenotypes observed in patients with FHC, we chose a common mutational site in the α -TM binding domain located at codon 92 (Figure 1a) (29,30). The R92Q mutation has been identified in 4 independent families presenting with FHC (28). A cardiac-specific transgenic construct was generated to express a murine cTnT molecule containing a dinucleotide change that results in the substitution of a single amino acid (R→Q) at codon 92 (Figure 1b; R92Q-Myc). Both the mutant and wild-type proteins are *myc*-tagged at their NH₂-termini. We have previously shown that the presence of the 11-amino acid *c-myc* epitope on the NH₂-terminus of the native murine cTnT molecule does not result in cardiac pathology (17).

The R92Q-Myc construct was used to generate 5 inde-

pendent lines of transgenic mice. Founder animals were identified by Southern analysis (data not shown). The addition of the 11-amino acid *c-myc* epitope to the 5' end of the cDNA construct generates a transgenic protein with a slightly slower mobility relative to endogenous cTnT in SDS-PAGE gels. This allows unambiguous identification of the transgene protein by Coomassie staining (Figure 2a). Myofibrils were isolated from 3 independent R92Q-Myc lines, a WT-Myc animal, and a nontransgenic (non-Tg) sibling. Equal amounts of myofibril proteins were loaded on an SDS-PAGE gel, and protein was detected by Coomassie staining. The transgene protein is clearly visible in all transgenic lanes (Figure 2a). Subsequent densitometry performed on a representative gel revealed that each transgenic line has a unique Tg-cTnT/endogenous-cTnT ratio. As has been previously noted in transgenic mouse models overexpressing contractile proteins, the level of endogenous cTnT protein is clearly decreased in response to increasing levels of transgene expression (31). Thus, each independent R92Q line can be distinguished by the relative level of endogenous cTnT replacement. Three representative lines were chosen for further study that express 30%, 67%, and 92% of their total cTnT as the transgenic form. To verify that the putative transgene band shown in Figure 2a did correspond to the R92Q-Myc protein, an identical set of SDS-PAGE gels was run, blotted onto nitrocellulose, and probed with either a *c-myc* (Figure 2b, top) or cTnT (Figure 2b, bottom) mAb. The cTnT mAb clearly detects both endogenous cTnT and the transgene, and again demonstrates the relative levels of replacement seen in the transgenic lines. Thus, all subsequent phenotypic comparisons between lines can be directly correlated to the dosage of R92Q-Myc protein. Even with very high transgene/endogenous cTnT ratios (including near-replacement of cTnT with the mutant form), the overall myofibrillar stoichiometry is not altered (Figure 2c).

As was previously noted, the R92Q mutation occurs at a site known to be involved in the interaction of the troponin complex with α -TM (29). Thus, it is important to determine whether the R92Q-Myc protein is able to incorporate into the native myofibril. Crude heart homogenates were isolated from transgenic and nontransgenic mice and subjected to low-speed centrifugation in low-salt conditions. Equal aliquots from each subsequent fraction were analyzed by Western blotting, and representative results are shown in Figure 2d. Myofibrillar proteins are known to pellet under these conditions, as can be seen in Figure 2d (top). Identical results are obtained with homogenates

isolated from either WT-Myc or the R92Q-Myc mice (Figure 2d, middle and bottom, respectively). Thus, neither the addition of the *c-myc* epitope alone (WT-Myc) nor the R92Q mutation results in any alteration in the ability of the transgenic proteins to associate with native myofibrils. In addition, indirect immunofluorescence on isolated adult cardiac myocytes using the *c-myc* mAb revealed a clear striated sarcomeric staining pattern (Figure 2e, top), which also indicates that the transgene proteins incorporate into the cardiac sarcomere.

R92Q-Myc mice demonstrate dose-dependent changes in chamber mass. One of the main characteristics that distinguishes cTnT-related FHC from the β -MyHC form is

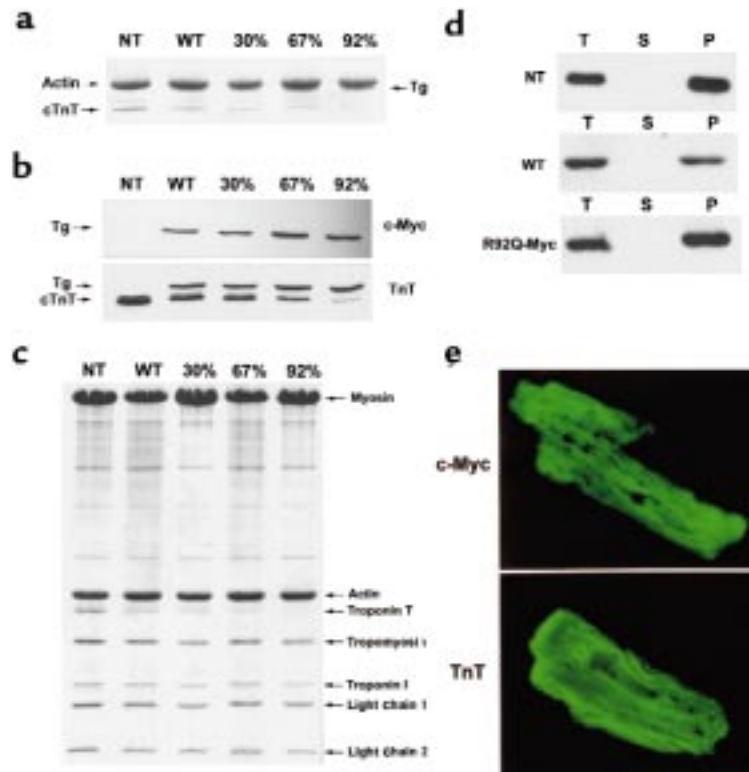


Figure 2

Expression of WT-Myc and R92Q-Myc proteins in cardiac tissue. (a) Coomassie-stained SDS-PAGE gel of myofibrils isolated from non-Tg (NT), WT-Myc (WT), and 3 independent R92Q-Myc lines. A total of 5 μ g myofibril protein was loaded per lane. Addition of the *c-myc* epitope tag decreases the mobility of the Tg protein (Tg) and allows unambiguous identification. Percentages (30%, 67%, 92%) represent Tg/endogenous cTnT ratios for the 3 R92Q-Myc lines. (b) Western blot analysis of myofibrils subjected to the same SDS-PAGE conditions as noted in a. Identical blots were probed with either a *c-myc* or cTnT mAb as indicated. The cTnT mAb detects both Tg and endogenous cTnT, and their relative positions are marked by arrows. The additional band immediately above the cTnT band (seen best in the NT lane) represents a known murine cTnT isoform. Note the progressive decrease in endogenous cTnT protein amounts among the 3 R92Q-Myc lines. (c) Myofibrils were purified from mouse hearts, subjected to SDS-PAGE, and Coomassie stained. Myofibrillar stoichiometry is maintained in all Tg lines. (d) Fractionation of cTnT. Three separate fractions were analyzed (T = total, S = supernatant, and P = pellet). Immunoblots of fractions from non-Tg (NT), WT-Myc (WT), and R92Q-67% (R92Q-Myc) were loaded for equal signal intensity and probed with either a cTnT (non-Tg) or *c-myc* (WT-Myc and R92Q-Myc) mAb as indicated. No Tg protein was detected in the S fraction for either WT-Myc or R92Q-Myc. (e) Transgene protein incorporation. Shown are confocal images of isolated adult cardiac myocytes probed with either *c-myc* (top; R92Q-67%) or TnT (bottom; non-Tg) mAb. $\times 4,300$.

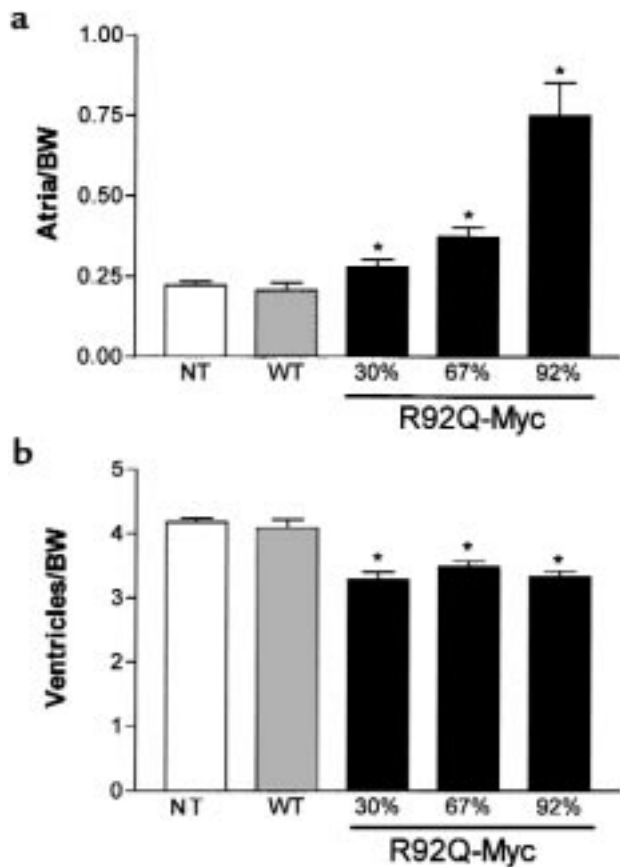


Figure 3 Heterozygous R92Q-Myc mice demonstrate decreased ventricular mass and dose-dependent changes in atrial mass. (a) Atrial weight/body weight ratios (milligram of chamber weight per gram of body weight [BW]) in 4- to 6-month-old animals. Error bars represent SEM. *P* values are vs. non-Tg (NT) animals (1-way ANOVA). (b) Ventricular weight/body weight ratios from the same mice as shown in a. **P* < 0.0001.

the degree of ventricular hypertrophy. Although there is phenotypic variation both between the different disease alleles and within affected families, most patients who are heterozygous for the cTnT mutations exhibit mild or no apparent ventricular hypertrophy (28). To determine whether the cardiac-specific expression of the R92Q-Myc protein would result in changes in cardiac mass, chamber weight/body weight ratios were compared among WT-Myc, all 3 lines of R92Q-Myc, and non-Tg sibling mice. Atrial hypertrophy was found in R92Q-Myc mice that was both progressive over time and increased proportionally with transgenic protein levels (Figure 3a). This increase in atrial mass was readily apparent at 4 weeks of age in the 92% R92Q-Myc line. Although both the left and right atria are affected, a clear left atrial predominance developed with increasing age and protein levels (data not shown). In contrast, ventricular mass decreased by approximately 18% in all 3 R92Q-Myc lines (Figure 3b). There was no variation in the degree of decrease in ventricular size between the 3 lines, and these findings are consistent in animals up to 1 year of age.

Myocytes isolated from R92Q-Myc hearts are smaller than either WT-Myc or non-Tg controls. To determine whether

the decrease in ventricular mass was reflected by a decrease in myocyte size, cells were isolated from the hearts of 67% R92Q mice and measured in the presence and absence of BDM. Subsequent video image analysis of ventricular myocytes incubated in the presence and absence of BDM yielded several very interesting results. BDM is known to disrupt force-producing cross-bridge formation in mammalian myocardium (32). An important finding of this analysis was that the mean area of R92Q myocytes was approximately 18% smaller than the areas of non-Tg or WT-Myc myocytes in the presence or absence of BDM (Table 1). However, R92Q-Myc cells are significantly longer and narrower in the presence of BDM. This observation is consistent with the idea that myocyte volume under isotonic conditions is reasonably stable, and with the observation that BDM-induced increases in cell length are accompanied by decreases in myocyte width (see later here). This difference in myocyte size provides an explanation for the observation that the ventricular mass of R92Q hearts is approximately 18% smaller than the mass of non-Tg hearts. ANOVA and inspection of the data in Table 1 clearly indicate that in quiescent cells, BDM elicits an increase in myocyte length and a decrease in midpoint myocyte width. BDM produces increases in mean myocyte length of less than 3% in non-Tg and WT-Myc cells, while producing an approximately 12% increase in the length of R92Q-Myc myocytes (Table 1). The ANOVA group × BDM interactions in the myocyte length and width data (Table 1) provide statistical verification that the effect of BDM on myocyte length and width is greatest in R92Q-Myc cells. In addition, no significant between-group differences in myocyte length were detected in the presence of BDM.

In a follow-up study, left ventricular myocytes were isolated from non-Tg and transgenic mice in order to determine the effects of transgene expression and BDM on sarcomere lengths. The results of these studies are summarized in Table 2. At baseline (–BDM), sarcomere lengths in the R92Q-Myc cells were shorter than those isolated from their non-Tg siblings. After treatment with 10 mM BDM, sarcomere lengths increased by 5% (non-Tg), 9.7% (R92Q-67%), and 12% (R92Q-92%). These results are consistent with the observed myocyte length increases (+BDM) of approximately 3%, 13%, and 15% for non-Tg, R92Q-67%, and R92Q-92%, respectively. Collectively, these data suggest that the basal level of contractile element activation in quiescent R92Q-Myc myocytes is abnormally high.

R92Q-Myc mice exhibit characteristic histopathological findings of FHC. The histopathological findings in FHC encompass a wide range of largely primary myocellular defects. The most common observations include myocellular disorganization, degeneration, and hypertrophy (19). In addition, many patients exhibit varying degrees of myocardial fibrosis and intimal thickening of small intramural arteries (33). The frequency and myocardial distribution of these findings vary widely and appear to reflect the clinical and genetic heterogeneity of the disease. Histological examination of cardiac sections from adult R92Q-Myc mice reveals a broad range of myocellular abnormalities (Figure 4, a–f). A representative section

from the R92Q-Myc-67% line is shown in Figure 4b and shows scattered hypertrophied cells and mild inflammation amid varying degrees of myocellular degeneration. Markedly pleiotrophic nuclei are also present. These regions are scattered primarily throughout the left ventricular free wall. Trichrome staining for collagen deposition reveals small areas of myocardial and perivascular fibrosis (Figure 4c). The degree and distribution of these findings are virtually identical between the 30% and 67% replacement lines. Although sections from R92Q-Myc-92% mice reveal qualitatively similar histopathology, it is much more severe and extensively distributed throughout the myocardium (Figure 4e). In particular, there are frequent foci of degenerating cardiac myocytes (note the hyperchromatic cells) and striking myocellular disarray. Evidence of myocyte necrosis and inflammatory change was also observed. Trichrome staining demonstrates widespread myocardial fibrosis in the higher-expressing 92% replacement line (Figure 4f). Cardiac sections from adult WT-Myc mice (Figure 4d) are indistinguishable from those from non-Tg controls (Figure 4a).

Ultrastructural analysis of R92Q-Myc hearts demonstrates allele-specific pathology. All the alleles that have been linked to FHC map to structural components of the cardiac sarcomere (2). To assess whether the incorporation of either the R92Q-Myc cTnT or our previously described cTnT-Myc-truncation protein would result in ultrastructural abnormalities at the level of the individual cardiac myocyte, electron microscopy was performed on hearts isolated from 5-week-old mice (Figure 5, a–f). Figure 5, a and b (non-Tg and WT-Myc, respectively), demonstrates normal sarcomeric structure, with full registration of Z bands and an ordered array of clearly defined thick and

Table 1
Isolated ventricular myocyte morphology

	Non-Tg	WT	R92Q	ANOVA Main effects
Length (μm)				Group
– BDM	123 \pm 3	122 \pm 3	105 \pm 2 ^A	BDM
+ BDM	126 \pm 3	125 \pm 3	120 \pm 2	Group \times BDM
Width (μm)				Group
– BDM	34 \pm 1	34 \pm 1	32 \pm 1	BDM
+ BDM	35 \pm 1	31 \pm 1 ^C	29 \pm 1 ^B	Group \times BDM
Area (μm^2)				Group
– BDM	3,029 \pm 92	2,931 \pm 102	2,421 \pm 77 ^A	Group
+ BDM	3,082 \pm 95	2,817 \pm 97	2,589 \pm 91 ^B	Group
Sample size (no. of myocytes)				
– BDM	100	100	90	
+ BDM	100	100	110	

ANOVA effects (main effects) at $P < 0.05$ and $P < 0.10$ (italics) levels: “Group” indicates a difference as a function of experimental group; “BDM” indicates that BDM affected the variable of interest; “Group \times BDM” interaction indicates that the effect of BDM on the variable of interest varied as a function of the group to which it was applied. Differences revealed in post hoc analysis: ^AR29Q vs. non-Tg and WT. ^BR29Q vs. non-Tg. ^CWT vs. non-Tg; all at $P < 0.05$ level.

thin filaments. Mitochondrial morphology, size, and number are all within normal limits. In contrast, sections from cTnT-Myc-truncation mice (Figure 5, c and d) reveal areas of focal myofibrillar lysis, misregistration of Z bands, and distinct regions of myofibrillar disarray. These findings are consistent with those found in patients with cardiomyopathies (34). Figure 5, e and f, shows representative sections from 2 independent lines of R92Q-Myc mice (67% and 92% replacement, respec-

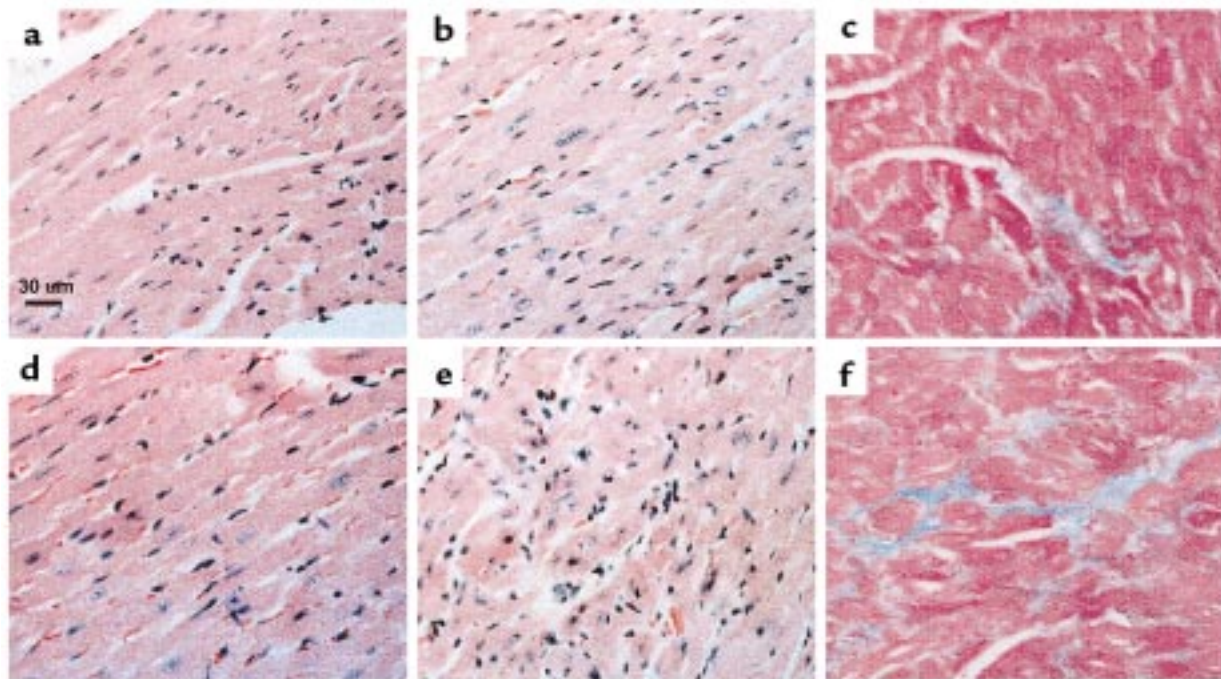
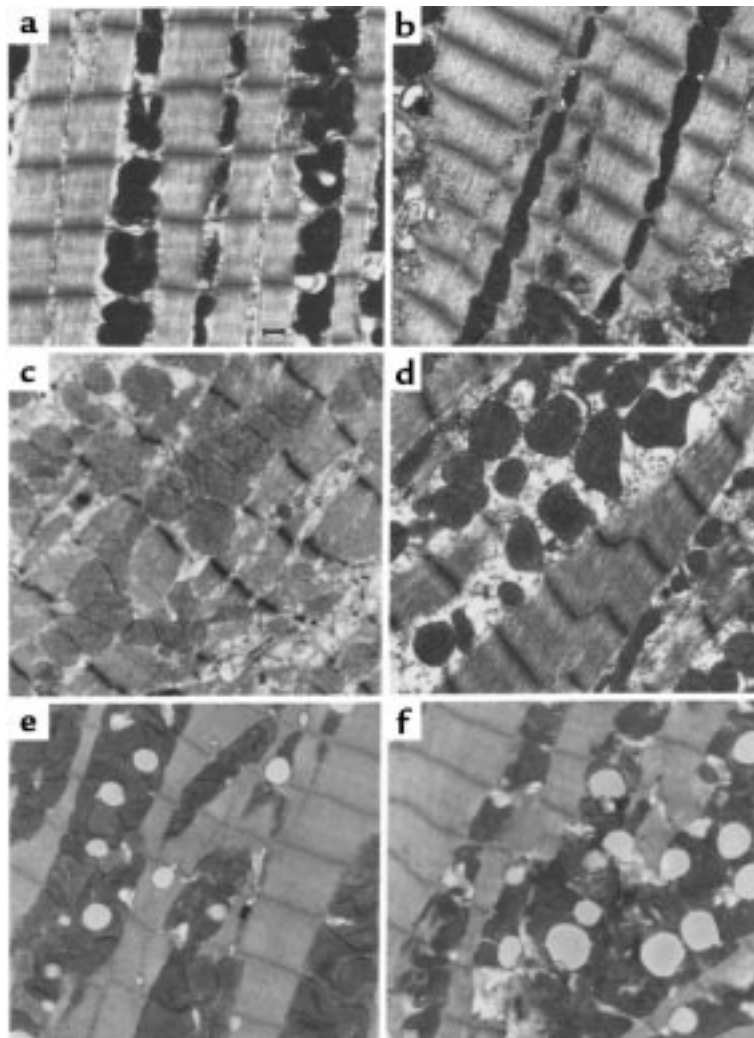


Figure 4
R92Q-Myc mice demonstrate myocellular disarray and fibrosis. Cardiac sections from 4- to 5-month-old non-Tg (a), R92Q-Myc-67% (b and c), WT-Myc (d), and R92Q-Myc-92% (e and f). a, b, d, and e were stained with hematoxylin and eosin. Note markedly pleiotropic nuclei and myocellular degeneration in b and e. e also demonstrates clear myocellular disarray and inflammation. c and f are stained with Masson's trichrome and demonstrate dose-dependent myocardial fibrosis. All panels $\times 400$.

Figure 5

Ultrastructural abnormalities in cTnT-related FHC mice are allele specific. Representative electron micrographs from left ventricular tissue isolated from non-Tg (a), WT-Myc (b), truncation-Myc (c and d), and R92Q-Myc (e and f) mice at 5 weeks of age. Sections from non-Tg and WT-Myc both demonstrate ordered arrays of myofibrils and normal mitochondrial morphology and number. Sections from 2 independent truncation-Myc lines reveal frequent misregistration of Z bands, myofibrillar disarray, and degeneration. Mitochondria are variable in size and morphology is normal. In comparison, both the R92Q-Myc lines (e = 67%, f = 92%) demonstrate largely preserved sarcomeric structure; however, note the lipid deposition and increased numbers of small mitochondria with loss of well-defined membranes and cristae. $\times 15,000$. Scale bar: 1 μm .



tively). Sarcomeric structure was found to be intact; thus, the incorporation of the mutant protein does not appear to have a direct deleterious effect on myofibrillar organization. However, the R92Q-Myc myocytes exhibited a striking degree of lipid deposition and increased numbers of mitochondria with evidence of mitochondrial degeneration. These findings are more prominent in the R92Q-Myc-92% line (compare Figure 5, e with f). In addition, frequent apoptotic nuclei can be seen in the higher-expressing line (data not shown). Taken together, these findings suggest that mutations in different functional domains within the cTnT molecule can lead to distinct phenotypes at the ultrastructural level and may form the basis for the varying phenotypes seen in cTnT-related FHC.

Expression of hypertrophic markers in R92Q-Myc mice. It is well established that the cardiac hypertrophic response is accompanied by a complex temporal array of changes in gene expression (35,36). As an initial step in characterizing the progression of the ventricular pathology at the molecular level, a series of Northern blot analyses were performed on total ventricular RNA isolated from all 3 R92Q-Myc lines, WT-Myc, and non-Tg sibling mice at several time points: 1.5, 4.5, and 8 months (Figure 6, a and b). Each blot was sequentially hybridized with the well-characterized markers of hypertrophy, ANF and β -MyHC. ANF is induced at high levels at very early time points in the R92Q-Myc-92% line and remain high at the

latest time point examined, 8 months of age (Figure 6b). Although ANF is also induced by 1.5 months in the 67% line, the initial degree of induction was smaller in magnitude and the levels seem to increase slowly over time, reaching a level equivalent to that seen in the 92% line by 8 months of age. Only low levels of ANF transcripts were found in RNA isolated from the 30% line, and this was not evident until 8 months of age. Similar results were seen with β -MyHC; however, there was a clear delay in the onset of marker induction between the 67% and 92% lines, with the 67% line demonstrating barely detectable β -MyHC mRNA by 4.5 months. In addition, unlike ANF, the induction of β -MyHC was clearly progressive over time in these 2 lines. No induction of β -MyHC was seen in the 30% line at any time point measured. No significant differences in β -MyHC or SERCA2 expression were found in any of the cTnT-Myc transgenic lines. No evidence for hypertrophic marker induction at any time point can be found in the WT-Myc or cTnT-Myc-truncation lines (see Figure 6b). Thus, it appears that as the degree of replacement of the normal cTnT protein with the R92Q-Myc form increases from 30% to 92%, both the magnitude and temporal expression of ANF and β -MyHC change in a transgene-specific pattern. This may well reflect a primary response of the ventricular myocyte to the degree of functional impairment caused

Table 2

Sarcomere length (μm) in isolated adult cardiac myocytes

	Non-Tg ^a	R92Q (67%)	R92Q (92%)
- BDM	1.82 \pm 0.02 (35)	1.65 \pm 0.02 ^b (34)	1.64 \pm 0.02 ^b (35)
+ BDM (10 mM)	1.92 \pm 0.01 ^c (25)	1.81 \pm 0.01 ^{b,c} (36)	1.82 \pm 0.01 ^{b,c} (30)

Values presented as mean \pm SEM. Values in parentheses represent the number of myocytes from which each mean was determined. ^aLittermate controls from the R92Q (67%) transgenic controls. ^bOne-way ANOVA analysis; significantly different relative to non-Tg ($P < 0.05$). ^cTwo-tailed t tests: - BDM different from + BDM ($P < 0.05$).

Table 3Means \pm SEM of measured cardiac parameters: Starling loading (100–600 mmHg \times mL/min)

	Non-Tg	R92Q-Myc (67%)	Percent change
Working heart	(n = 6, 53)	(n = 6, 49)	
Heart rate (beats per min)	425 \pm 4	426 \pm 3	Paced
+dP/dT (mmHg/s)	6,161 \pm 198	7,288 \pm 243	+18 ^A
-dP/dT (mmHg/s)	4,023 \pm 126	3,233 \pm 66	-20 ^A
LVP (mmHg)	102 \pm 3	108 \pm 2	+6
Time to peak (ms)	44 \pm 1	31 \pm 1	-30 ^A
Time to 50% relaxation (ms)	30 \pm 1	30 \pm 1	0
Tau (ms)	28 \pm 2	66 \pm 9	+136 ^A

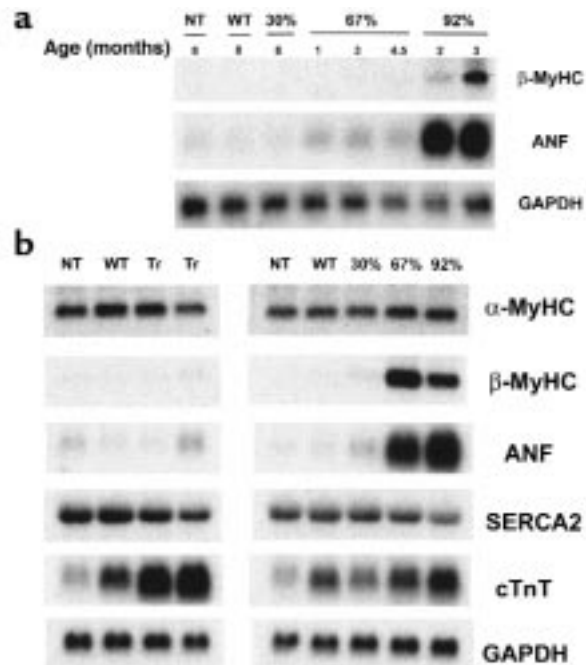
^AP < 0.001 transgenic vs. control; unpaired Student's *t* test.

by the presence of increasing amounts of R92Q-Myc protein within the cardiac sarcomere.

Functional analysis of R92Q-Myc mice reveals hypercontractility and diastolic dysfunction. Patients with FHC demonstrate a wide range of cardiovascular physiological profiles. Symptoms consistent with diastolic dysfunction are commonly seen and have previously been at least partially attributed to the degree of ventricular hypertrophy (19). Patients also frequently demonstrate marked hypercontractile systolic function, and treatment with negative inotropic medications is a mainstay of clinical management (36). The cause of the observed hypercontractility, however, remains unclear. To gauge the functional effects of the R92Q-Myc protein on whole-heart hemodynamics, an isolated work-performing model was used (37). The data presented here derive from the R92Q-Myc-67% mice. We also attempted to analyze the R92Q-Myc-92% hearts, but the profound atrial enlargement prevented successful preparations. The R92Q-Myc-67% hearts exhibited significantly higher intrinsic heart rates than age-matched non-Tg siblings (~425 vs. 370 beats per minute). Thus, to control for chronotropic differences in contractile function, both transgenic and non-Tg hearts were paced at 425 beats per minute in all subsequent experiments. Systolic (+dP/dT) and diastolic (-dP/dT) performance were assessed by increasing volume (venous return), thus varying cardiac minute workload from 250 to 600 mmHg \times mL/min in a stepwise fashion. A summary of hemodynamic data is shown in Table 3. The R92Q-Myc-67% hearts produce maximal rates of pressure development (+dP/dT) that are significantly increased (+18%) relative to controls at similar workloads. This increase in systolic function is also reflected in a significant decrease (-30%) in the time required to reach peak intraventricular pressure (TPP). Careful examination of the relaxation indices -dP/dT, RT_{1/2} (time to 50% relaxation), and Tau (time constant of ventricular relaxation) reveals a clear impairment of diastolic function in R92Q-Myc hearts. The diastolic dysfunction is largely restricted to the early diastolic/late phase of relaxation (represented by the significant increase (+136% in Tau), whereas the initial "fast" phase of the diastolic pressure drop is unaffected (RT_{1/2}). The net effect would be a prolongation of isovolumic relaxation with a higher potential for early activation. In patients with hypertrophic cardiomyopathy, prolongation of isovolumic relaxation is a relatively common finding that has largely been attrib-

uted to the presence of hypertrophy and nonuniformity (38). Another proposed mechanism is abnormal Ca²⁺ handling. Because the R92Q-Myc-67% mice do not demonstrate ventricular hypertrophy, we believe that the observed diastolic dysfunction is secondary to either Ca²⁺ hypersensitivity (due to the increased sarcomeric activation) or an alteration in Ca²⁺ homeostasis within the cardiac myocyte. Thus, the R92Q-Myc-67% mice exhibit 2 of the most common clinical findings in patients with FHC: hypercontractility and diastolic dysfunction.

Isolated R92Q-Myc cardiac myocytes demonstrate impaired relaxation. To determine whether contractile function in the isolated working heart was reflected at the level of the cardiac myocyte, cellular contractility studies were performed on isolated cells from non-Tg, WT-Myc, and R92Q-Myc-67% mice. The extent of myocyte shortening, both in absolute and relative terms, tends to be smaller in R92Q-Myc myocytes (Table 4). During pacing, myocyte-shortening rate and velocity are both significantly slower in myocytes from R92Q-Myc mice. Relative to both non-Tg and WT-Myc cells, myocyte relaxation and overall contraction times are prolonged in R92Q-Myc cells (Table 4 and Figure 7). Taken at face value, these data are indicative of impaired myocyte contraction and relaxation. The

**Figure 6**

Induction of hypertrophic markers in R92Q-Myc mice. (a) Induction time-course Northern blot analysis of total ventricular RNA isolated from non-Tg (NT), WT-Myc (WT), and all 3 R92Q-Myc Tg lines. Age at time of RNA isolation is noted for each lane. The blot was serially hybridized with a radiolabeled β -MyHC oligonucleotide probe and ANF and GAPDH cDNA probes as described in Methods. (b) Northern blot analysis of total ventricular RNA isolated from non-Tg (NT), WT-Myc (WT), truncation-Myc (Tr), and all 3 R92Q-Myc Tg lines. A total of 10 μ g of total RNA was loaded per lane. The blot was serially hybridized with α -MyHC and β -MyHC oligonucleotide probes, followed by ANF, SERCA2, cTnT, and GAPDH cDNA probes. Note that the cTnT probe detects both endogenous (as seen in NT lanes) and transgene transcripts.

latter observation at the single-cell level is consistent with the results of the isolated working heart data, whereas the former observation is not. However, mean resting sarcomere lengths in the R92Q-Myc myocytes were significantly shorter than in the WT-Myc myocytes. As mentioned earlier, this difference may have been reflective of a higher basal level of contractile element activation in the R92Q myocytes. The shorter sarcomere lengths in the R92Q-Myc cells would be expected to have a suppressive effect on myocyte shortening, because contractions would be elicited at less optimal sarcomere lengths and against a stronger passive restoring force (see Discussion). Finally, significant differences between non-Tg and WT-Myc are only observed in time to peak shortening and time to 50% relengthening. This illustrates the utility of including a WT-Myc control in this type of experiment.

Discussion

In this study, we present evidence that the expression of a cTnT FHC allele, R92Q, in the mouse heart results in a complex cardiovascular phenotype that exhibits both similarities and differences relative to a previously described mouse model expressing a truncated FHC-related cTnT allele (17). Although these 2 models demonstrate some phenotypic overlap (particularly with regard to decreased left ventricular mass), they remain distinct at several levels, which we believe directly reflects the degree of functional impairment of the cTnT protein and may well provide insight into the molecular pathogenesis of this complex disorder.

Since the identification of the first disease-related allele in 1990, it has become clear that the broad range of clinical phenotypes is matched by a striking genetic

heterogeneity. The clinical phenotypes vary both within and among the numerous disease alleles and may well reflect the varied structural and functional roles of the contractile proteins within the cardiac myocyte. It has been noted that the cTnT-related FHC alleles result in a particularly malignant clinical phenotype whereby approximately 50% of affected patients experience sudden cardiac death by the third decade of life (30).

Despite the absence of ventricular hypertrophy in the R92Q mice, the 2 higher-expressing lines (67% and 92%) demonstrate significant induction of both ANF and β -MyHC transcripts. Both the timing of onset and magnitude of the induction are distinct between all 3 lines. In comparison, the previously described Myc-truncation lines do not exhibit induction of hypertrophic markers at identical time points. While the underlying mechanisms are unknown, the timing of the onset of hypertrophic marker expression in the R92Q-Myc lines does appear to correlate with both the extent and severity of the later pathological findings (e.g., fibrosis), thus providing a qualitative marker for the progression of pathology in this model system. None of these markers is induced in the TnT-truncation mice, where myocellular disarray is common but fibrosis is rare, suggesting that expression of these genes may be related to fibrosis.

The ultrastructural findings in hypertrophic cardiomyopathy are quite varied and include decreased mitochondrial size, myofibrillar lysis, changes in Z-band morphology, and myofibrillar disorientation (34–39). No relationship between morphological changes and cardiac functional status has been identified (40). These studies, however, were performed before the availability of genotype analysis for FHC; thus, no information is currently available regarding allele- or gene-specific ultrastructural findings. Ultrastructural examination of cardiac tissues from 5-week-old R92Q-Myc mice reveals early cellular changes. The R92Q-Myc-67% myocytes demonstrate scattered areas of disorganization, lipid deposition, and mitochondrial degeneration. The findings in the higher-expressing R92Q-Myc-92% lines are largely similar yet more extensive, and evidence of myocyte apoptosis is also observed (data not shown). Of note, sarcomere structure is largely preserved. Although the mechanism underlying these findings is unknown, both lipid deposition and mitochondrial lysis are commonly seen in ischemic cardiac tissue (41,42). One possibility is that the increased level of basal sarcomeric activation observed in R92Q-Myc myocytes has led to a chronic increase in oxygen demand (MVO_2) that, over time, results in the ultrastructural changes we have observed. Experiments to test this hypothesis are in progress.

The R92Q-Myc ultrastructural findings are in stark contrast to those seen in the Myc-truncation myocytes, and these differences may well represent the effects of the primary cTnT mutation on the cardiac sarcomere. The incorporation of less than 6% of total cTnT as the truncated form led to focal myofibrillar lysis and misregistration of Z bands. Mitochondrial structure was normal, and no lipid deposition was observed in the Myc-truncation lines. The cTnT-truncation molecule has effectively lost a significant portion of the 3' TnI-TnC-TM binding site and would likely result in a troponin complex that exhibits an altered Ca^{2+}

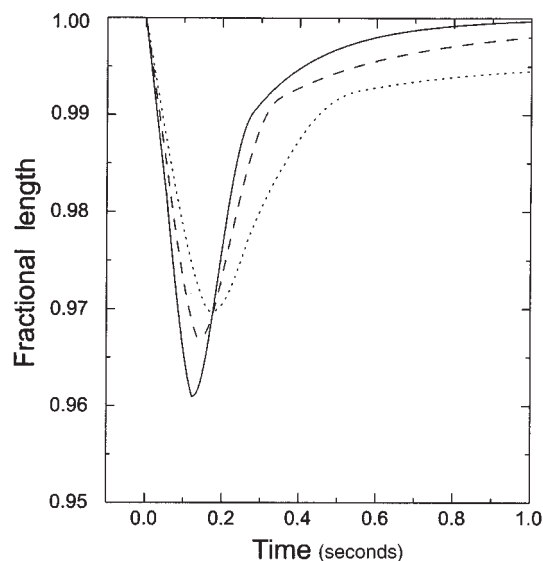


Figure 7

Representative ventricular myocyte-shortening dynamics. Non-Tg (solid line), WT-Myc (dashed line), and R92Q-Myc (dotted line) are shown above. “Fractional length” (ordinate label) refers to cell shortening as a fraction of resting cell length. Myocyte-shortening dynamics for each cell type were reconstructed from the data presented in Table 1 (and mean times to 25%, 75%, and 90% relengthening; not reported in Table 1) by interpolation.

Table 4

Isolated ventricular myocyte-shortening characteristics

	Non-Tg	WT	R92Q	ANOVA Main effect	Post hoc contrasts
Resting length (μm)	118 \pm 3	119 \pm 3	102 \pm 2	$P < 0.05$	b, c
Myocyte shortening (μm)	4.6 \pm 0.5	3.9 \pm 0.3	3.1 \pm 0.2	$P < 0.05$	b
Fractional shortening (% resting cell length)	3.9 \pm 0.3	3.3 \pm 0.2	3.0 \pm 0.2	$P < 0.10$	
Time to peak shortening (ms)	122 \pm 27	137 \pm 28	162 \pm 40	$P < 0.05$	a, b, c
Maximal shortening velocity, $-dS/dT_{\text{max}}$ ($\mu\text{m/s}$)	-79 \pm 7	-66 \pm 6	-47 \pm 4	$P < 0.05$	b, c
Maximal shortening rate (s^{-1})	-17.7 \pm 0.3	-16.7 \pm 0.2	-15.2 \pm 0.4	$P < 0.05$	b, c
Maximal relengthening velocity, $+dS/dT_{\text{max}}$ ($\mu\text{m/s}$)	44 \pm 6	36 \pm 4	19 \pm 3	$P < 0.05$	b, c
Maximal relengthening rate (s^{-1})	8.3 \pm 0.4	8.5 \pm 0.3	5.9 \pm 0.5	$P < 0.05$	b, c
Time to 50% relaxation (ms)	217 \pm 6	259 \pm 8	362 \pm 12	$P < 0.05$	a, b, c
Sample size (no. of cells)	67	63	73	-	-

Post hoc contrasts ($P < 0.05$): a, WT vs. non-Tg; b, R92Q vs. non-Tg; c, R92Q vs. WT.

sensitivity. Incorporation of this “on” or “off” protein may lead to local stresses within the sarcomere and result in structural breakdown. In comparison, the R92Q-Myc mutation represents a single-amino acid substitution in the Myc-truncation binding site of cTnT. As we have shown, this mutation does not affect the ability of the transgenic protein to incorporate into the myofibril. Recent cTnT exchange experiments using a permeabilized rabbit cardiac muscle fiber system have shown that incorporation of a human R92Q cTnT molecule leads to an increase in Ca^{2+} sensitivity without altering the maximally activated fiber tension (14). Thus, the R92Q-Myc mutation may act as a “change-in-function” allele rather than the “poison polypeptide” truncation mutation, and this difference may be reflected in the ultrastructural findings.

A major advantage of using a transgenic approach to study the functional effects of point mutations on contractile proteins is the ability to directly correlate in vitro findings to whole-heart contractility. Studies performed on adult cardiac myocytes isolated from WT-Myc, R92Q-Myc, and non-Tg hearts suggest that the presence of the R92Q point mutation results in a higher basal level of sarcomeric activation. In the present experiments, inhibiting the actomyosin cross-bridges by incubating the cells in BDM elicited a markedly greater increase in cell length in the R92Q-Myc myocytes compared with either control group. The mechanism that underlies this increase in contractile element activation is currently unknown. One possible explanation is that the substitution of glutamine for the positively charged arginine at cTnT codon 92 alters the interaction between TM and the troponin complex, such that cross-bridge formation occurs at a lower $[\text{Ca}^{2+}]$. Although the verification of this “partial activation” model awaits the availability of the high-resolution crystal structure of cTnT, the end effect would be an apparent increase in Ca^{2+} sensitivity. This hypothesis is supported by the findings of Morimoto et al. (14), wherein the exchange of a human R92Q-cTnT

molecule into permeabilized rabbit cardiac muscle fibers resulted in a clear decrease in the free $[\text{Ca}^{2+}]$ required for tension generation.

The subsequent effects on cardiac contractility caused by this elevation in the basal level of sarcomeric activation would be expected to be complex. As a first step in addressing this issue, we examined the shortening characteristics of isolated adult cardiac myocytes from R92Q-Myc, WT-Myc, and non-Tg animals. The expectation would be that the increase in contractile protein activation would lead to a concomitant increase in contractility due to heightened cross-bridge formation at submaximal Ca^{2+} . The R92Q-Myc myocytes, however, exhibited a decrease in both maximal shortening velocity ($-dS/dT_{\text{max}}$) and maximal shortening rate constant, which is suggestive of a decrease in overall contractility. These data, however, must be interpreted in the context of the observed shorter myocyte and sarcomere lengths at baseline in R92Q-Myc myocytes. The shorter basal sarcomere lengths in the R92Q-Myc cells would be expected to have suppressive effect on myocyte shortening for 2 reasons. First, contraction in R92Q-Myc myocytes was initiated at shorter (less optimal) sarcomere lengths in contrast to WT-Myc cells. Second, the extent of myocyte shortening is determined by the interaction between an active contractile process that generates force and promotes shortening and a passive restoring force that resists shortening. Because intrinsic myocyte length is not different between experimental groups when the actin cross-bridge interaction is inhibited by BDM, it is likely that contraction of R92Q-Myc cells is initiated against a greater restoring force, which would, in turn, directly oppose active myocyte shortening. Thus, the slower measured contractile indices are not necessarily reflective of the active contraction status of the R92Q-Myc myocytes. In contrast, the increased basal level of contractile element activation found in

R92Q-Myc myocytes would be expected to have a depressive effect on relaxation in that the threshold for inhibition of cross-bridge formation would be increased. Our data support this hypothesis in that both the maximal relengthening velocity (+dS/dT_{max}) and the maximal relengthening rate constant are significantly decreased in R92Q-Myc myocytes compared with both the WT-Myc and non-Tg controls.

Our isolated cardiac myocyte data represent the effects of a primary alteration in sarcomeric function on single-cell contractility. These findings are clearly reflected in the subsequent physiological effects seen at the whole-heart level. Hearts isolated from R92Q-Myc-67% animals and subjected to a stepwise increase in cardiac workload exhibit both hypercontractility and impaired relaxation compared with non-Tg littermates. In contrast, hearts isolated from Myc-truncation mice demonstrated impairment of both systolic and diastolic function. This again illustrates an important distinction between the 2 models that we believe reflects on the nature of the primary mutation. In many cases of humans with FHC, the severity of the symptoms correlates to the degree of left ventricular hypertrophy, with a decrease in compliance leading to increased filling pressures and worsening of symptoms over time (19). It has long been noted, however, that in some cases the clinical symptoms are clearly out of proportion to the degree of hypertrophy. This “cellular diastolic dysfunction” is thought to be due to changes in Ca²⁺ handling at the level of the cardiac myocyte, and is supported by our findings in that both cTnT-Myc animal models exhibit diastolic dysfunction in the absence of ventricular hypertrophy. Although another common noninvasive clinical finding in FHC patients is cardiac hypercontractility, the underlying cause remains unclear. We believe that the observed hypercontractility in the R92Q-Myc-67% mice is a direct result of the basal increase in contractile element activation observed in the isolated cell studies. Thus, the characterization of the R92Q-Myc transgenic mice results in findings that are internally consistent from the level of the point mutation in a single sarcomeric protein to the resultant physiology at the whole-heart level.

One of the most basic questions regarding the pathogenesis of cTnT-related FHC in patients is the actual mechanism of the observed sudden death. It is again important to note that patients with cTnT-related FHC tend to exhibit mild or no ventricular hypertrophy, yet experience a high frequency of sudden death at an early age. This suggests that the primary effects of the point mutation act at the level of the cardiac myocyte. Indeed, the issue of a cellular phenotype for one of the β-MyHC-related FHC mouse models was recently addressed in an interesting report by Spindler et al. (43), wherein they documented changes in cardiac energetics (specifically decreased [PCr]) in hearts isolated from αMHC403/+ mice. This report represents the first opportunity to examine 2 different disease alleles within the same gene. The striking differences exhibited by the mice expressing the 2 mutations have made it possible to conclude that many of the phenotypes can exist in the absence of others. For example, disarray can exist without fibrosis, and diastolic dysfunction can occur in

the absence of hypertrophy. In addition, the analyses of isolated cells and the intact heart have provided new insight into the mechanisms of pathogenesis of FHC.

Acknowledgments

This work was supported by grants from the National Institutes of Health (HL-50560 to L.A. Leinwand; HL-060546 to J. Robbins; and HL-40306 to R.L. Moore). The authors thank Yvonne Kress for electron micrographs, Ed Yellin for discussions about diastolic dysfunction (both of Albert Einstein College of Medicine, Bronx, New York, USA), Murali Chandra and R. John Solaro for discussions about TnT (University of Illinois, Chicago, Illinois, USA), Kurt Haubold for confocal microscopy, and Jill Jones for help in manuscript and figure preparation (both of University of Colorado, Boulder, Colorado, USA).

1. Towbin, J. 1998. The role of cytoskeletal proteins in cardiomyopathies. *Curr. Opin. Cell Biol.* **10**:131–139.
2. Watkins, H., Seidman, J.G., and Seidman, C.E. 1995. Familial hypertrophic cardiomyopathy: a genetic model of cardiac hypertrophy. *Hum. Mol. Genet.* **4**:1721–1727.
3. Sweeney, H.L., Straceski, A.J., Leinwand, L.A., and Faust, L. 1994. Heterologous expression of a cardiomyopathic myosin that is defective in its actin interaction. *J. Biol. Chem.* **269**:1603–1605.
4. Sara, M., and Ikebe, M. 1996. Functional analysis of the mutations in the human cardiac β-myosin that are responsible for familial hypertrophic cardiomyopathy. *J. Clin. Invest.* **98**:2866–2873.
5. Roopnarine, O., and Leinwand, L.A. 1998. Functional analysis of myosin mutations that cause familial hypertrophic cardiomyopathy. *Biophys. J.* **75**:3023–3030.
6. Vikstrom, K.L., Factor, S.M., and Leinwand, L.A. 1996. Mice expressing mutant myosin are a model for hypertrophic cardiomyopathy. *Mol. Med.* **2**:556–567.
7. Geisterfer-Lowrance, A.A.T., et al. 1996. A mouse model of familial hypertrophic cardiomyopathy. *Science.* **272**:731–734.
8. Tobacman, L.S. 1996. Thin filament-mediated regulation of cardiac contraction. *Annu. Rev. Physiol.* **58**:447–481.
9. Perry, S.V. 1998. Troponin T: genetics, properties and function. *J. Muscle Res. Cell Motil.* **19**:575–602.
10. Thierfelder, L., et al. 1994. α-Tropomyosin and cardiac troponin T mutations cause familial hypertrophic cardiomyopathy: a disease of the sarcomere. *Cell.* **77**:701–712.
11. Watkins, H., Seidman, C.E., Seidman, J.G., Feng, H.S., and Sweeney, H.L. 1997. Expression and functional assessment of a truncated cardiac troponin T that causes hypertrophic cardiomyopathy. *J. Clin. Invest.* **98**:2456–2461.
12. Marian, A.J., Zhao, G., Seta, Y., Roberts, R., and Yu, Q.-T. 1997. Expression of a mutant (Arg⁹²Gln) human troponin T, known to cause hypertrophic cardiomyopathy, impairs adult cardiac myocyte contractility. *Circ. Res.* **81**:76–85.
13. Lin, D., Bobkova, A., Homsher, E., and Tobacman, L.S. 1996. Altered cardiac troponin T in vitro function in the presence of a mutation implicated in familial hypertrophic cardiomyopathy. *J. Clin. Invest.* **97**:2842–2848.
14. Morimoto, S., Yanaga, F., Minakami, R., and Ohtsuki, I. 1998. Ca²⁺-sensitizing effects of the mutations at Ile-79 and Arg92 of troponin T in hypertrophic cardiomyopathy. *Am. J. Physiol.* **275**:C200–C207.
15. Cuda, G., Fananapazir, L., Epstein, N.D., and Sellers, J.R. 1997. The in vitro motility activity of β-cardiac myosin depends on the nature of the β-myosin heavy chain gene mutation in hypertrophic cardiomyopathy. *J. Muscle Res. Cell Motil.* **18**:275–283.
16. Sweeney, H.L., Feng, H.S., Yang, Z., and Watkins, H. 1998. Functional analyses of troponin T mutations that cause hypertrophic cardiomyopathy: insights into disease pathogenesis and troponin function. *Proc. Natl. Acad. Sci. USA.* **95**:14406–14410.
17. Tardiff, J.C., et al. 1998. A truncated cardiac troponin T molecule in transgenic mice suggests multiple cellular mechanisms for familial hypertrophic cardiomyopathy. *J. Clin. Invest.* **101**:2800–2811.
18. Oberst, L., et al. 1998. Dominant-negative effect of a mutant cardiac troponin T on cardiac structure and function in transgenic mice. *J. Clin. Invest.* **102**:1498–1505.
19. Maron, B.J., Bonow, R.O., Cannon, R.O., Leon, M.B., and Epstein, S.E. 1987. Hypertrophic cardiomyopathy. Interrelations of clinical manifestations, pathophysiology, and therapy. Part I. *N. Engl. J. Med.* **316**:780–789.
20. Lawson, J.W. 1998. Hypertrophic cardiomyopathy: current views on etiology, pathophysiology, and management. *Am. J. Med. Sci.* **294**:191–210.
21. Evan, G.I., Lewis, G.K., Ramsey, G., and Bishop, J.M. 1985. Isolation of

- monoclonal antibodies specific for human *c-myc* proto-oncogene product. *Mol. Cell. Biol.* **5**:3610–3616.
22. Tantravahi, J., Alvira, M., and Falck-Pedersen, E. 1993. Characterization of the mouse β^{maj} globin transcription termination region: a spacing sequence is required between the poly(A) signal sequence and multiple downstream termination elements. *Mol. Cell. Biol.* **13**:578–587.
 23. Hogan, B., Constantini, F., and Lacy, E. 1986. *Manipulating the mouse embryo: a laboratory manual*. Cold Spring Harbor Press. Cold Spring Harbor, NY. 1–487.
 24. Chomczynski, P., and Sacchi, N. 1987. Single-step method of RNA isolation by acid guanidinium thiocyanate-phenol-chloroform extraction. *Anal. Biochem.* **162**:156–169.
 25. Wolska, B.M., and Solaro, R.J. 1997. Method for isolation of adult mouse cardiac myocytes for studies of contraction and microfluorimetry. *Am. J. Physiol.* **271**:H1250–H1255.
 26. Stuafter, B.L., Palmer, B.M., Hazel, A., Cheung, J.Y., and Moore, R.L. 1997. Hypertension alters rapid cooling contractures in single rat cardiocytes. *Am. J. Physiol.* **271**:C1000–C1006.
 27. Williams, J.L., Hathaway, C.A., Kloster, K.L., and Layne, B.H. 1997. Low power, type II errors and other statistical problems in recent cardiovascular research. *Am. J. Physiol.* **273**:H487–H493.
 28. Watkins, H., et al. 1995. Mutations in the genes for cardiac troponin T and α -tropomyosin in hypertrophic cardiomyopathy. *N. Engl. J. Med.* **332**:1058–1064.
 29. Forissier, J.F., et al. 1996. Codon 102 of the cardiac troponin T gene is a putative hot spot for mutations in familial hypertrophic cardiomyopathy. *Circulation.* **94**:3069–3073.
 30. Moolman, J.C., et al. 1997. Sudden death due to troponin T mutations. *J. Am. Coll. Cardiol.* **29**:549–555.
 31. Gulick, J., et al. 1997. Transgenic remodeling of the regulatory myosin light chains in the mammalian heart. *Circ. Res.* **80**:655–664.
 32. Gwathmey, J.K., Hajjar, R.J., and Solaro, R.J. 1991. Contractile deactivation and uncoupling of cross-bridges: effects of 2,3-butanedionemoxime on mammalian myocardium. *Circ. Res.* **69**:1280–1292.
 33. Davies, M.J., and McKenna, W. 1995. Hypertrophic cardiomyopathy: pathology and pathogenesis. *Histopathology.* **26**:493–500.
 34. Maron, B.J., Ferrans, V.J., and Roberts, W.C. 1975. Ultrastructural features of degenerated cardiac muscle cells in patients with cardiac hypertrophy. *Am. J. Pathol.* **79**:387–434.
 35. Vikstrom, K.L., Bohlmeier, T., Factor, S.M., and Leinwand, L.A. 1998. Hypertrophy, pathology and molecular markers of cardiac pathogenesis. *Circ. Res.* **82**:773–778.
 36. Schaub, M.C., Hefti, M.A., Harder, B.A., and Eppenberger, H.M. 1997. Various hypertrophic stimuli induce distinct phenotypes in cardiomyocytes. *J. Mol. Med.* **75**:901–920.
 37. Grupp, I.L., Subramaniam, A., Hewett, T.E., Robbins, J., and Grupp, G. 1993. Comparison of normal, hypodynamic, and hyperdynamic mouse hearts using isolated work-performing heart preparations. *Am. J. Physiol.* **265**:H1401–H1410.
 38. Betocchi, S. Hess, O.M., Losi, M.A., Nonogi, H., and Krayenbuehl, H.P. 1993. Regional left ventricular dynamics in hypertrophic cardiomyopathy. *Circulation.* **88**:2206–2214.
 39. Tashiro, A., Masuda, T., and Segawa, I. 1990. Morphometric comparison of mitochondria and myofibrils of cardiomyocytes between hypertrophic and dilated cardiomyopathies. *Virchows Arch. A Pathol. Anat. Histopathol.* **416**:473–478.
 40. Baandrup, U., Florio, R.A., Roters, F., and Olsen, E.G. 1981. Electron microscopic investigation of endomyocardial biopsy samples in hypertrophy and cardiomyopathy. A semiquantitative study in 48 patients. *Circulation.* **63**:1289–1298.
 41. Greve, G., Rotevatn, S., Svendby, K., and Grong, K. 1990. Early morphologic changes in cat heart muscle cells after acute coronary artery occlusion. *Am. J. Pathol.* **136**:273–283.
 42. Miyazima, K., et al. 1991. Ischemic myocardial mitochondrial function and ultrastructural change: influence of regional myocardial blood flow. *Jpn. Circ. J.* **55**:714–720.
 43. Spindler, M., et al. 1998. Diastolic dysfunction and altered energetics in the $\alpha\text{MHC}^{403/+}$ mouse model of familial hypertrophic cardiomyopathy. *J. Clin. Invest.* **101**:1775–1783.